

ANALYSIS OF LUMPED PARAMETER MODELS FOR BLOOD FLOW SIMULATIONS AND THEIR RELATION WITH 1D MODELS

VUK MILIŠIĆ AND ALFIO QUARTERONI ¹

Abstract. This paper provides new results of consistence and convergence of the lumped parameters (ODE models) toward one-dimensional (hyperbolic or parabolic) models for blood flow. Indeed, lumped parameter models (exploiting the electric circuit analogy for the circulatory system) are shown to discretize continuous 1D models at first order in space. We derive the complete set of equations useful for the blood flow networks, new schemes for electric circuit analogy, the stability criteria that guarantee the convergence, and the energy estimates of the limit 1D equations.

1991 Mathematics Subject Classification. 35M20, 35L50, 65L05, 76Z05, 47H10.

1. INTRODUCTION

The cardiovascular system can be regarded as a wide hydraulic network under the action of a pulsatile pump. Different behavior can be observed at various locations of the closed loop. For instance in the arterial tree, the wave propagation is of greater influence while in the capillary bed, the flow is almost steady, putting into evidence the lumped character of the system. On the other hand, local phenomena, like anastomosis for instance, create flow perturbations upwardly and downwardly. This shows the interdependency of different scales of the system, leading to a multiscale approach.

Some simplified models take into account the previous properties of the cardiovascular system. For instance the Windkessel and similar lumped models are often used to represent blood flow and pressure in the arterial system ([1, 21, 30, 16]). These lumped models can be derived from electrical circuit analogies where current represents arterial blood flow-rate and voltage represents arterial pressure. Resistances represent arterial and peripheral resistance that occur as a result of viscous dissipation inside the vessels, capacitors represent volume compliance of the vessels that allows them to store large amounts of blood, and inductors represent inertia of the blood. The idea for the Windkessel model was originally put forward by Stephen Hales in 1733 [13] and further developed by Otto Frank in 1899 [11]. Frank used the Windkessel model to describe blood flow in the heart and systemic arteries. The analogy starts at the left ventricle where the blood pressure varies from a low of nearly zero to a high of approximately 120 mmHg and continues into the aorta and the systemic arteries where the pressure variation is significantly lower because of the elasticity of the large systemic arteries. This

²vuk.milisic@epfl.ch

³alfio.quarteroni@epfl.ch

Keywords and phrases: multiscale modelling, parabolic equations, hyperbolic systems, lumped parameters models, blood flow modelling

¹ Chair of Modelling and Scientific Computing, IACS, École Polytechnique Fédérale de Lausanne 1015 Lausanne, Switzerland

analogy resulted in the development of the original (two-element) Windkessel model comprising an electrical circuit with one resistor and one capacitor. Even though the model was originally derived for the ventricle and the aorta it can also be used for modelling the entire arterial tree; in this case the capacitor represents the compliance of the large arteries while the resistor represents the resistance of the small arteries and arterioles. However, when the model is used for the systemic arteries it is not able to reproduce realistic pressure profiles when the aortic blood flow is used as an input [26]. Therefore the Windkessel model was expanded [31] by adding a third term (a second resistor added in parallel with the capacitor) representing the resistance of the aorta. This version of the model is often referred to as the three-element Windkessel model or the modified Windkessel model. It is widely used and it is able to reproduce realistic flow-rate and pressure wave profiles as well as to fit experimental data [31]. Further expansions of the Windkessel model into a four-element model have proven to be even more reliable. In addition to the two resistors and the capacitor of the three-element Windkessel model, the four-element model comprises an inductor which accounts for blood inertia [26]. Besides being of simple derivation, the main advantage of lumped models is that they are easy to solve since they give rise to simple ordinary differential equations.

On the other hand, one dimensional models of the human arterial system were introduced by Euler in 1775, see [8]. They yield partial differential equations expressing the conservation of mass and momentum for inviscid flow. The wave propagation in the arterial flow was first described rigorously by Young in 1808, who derived the wave speed using an argument based on intuition and analogy to Newton’s theory of the speed of sound in air. In 1860, Riemann provided the analytical tools for the general equations when he introduced the method of characteristics, which was first applied to arterial flow by Anliker and co-workers [28] and Skalak [23]. Afterward, one dimensional models were extensively used to predict pressure and flow in the systemic tree, in various configuration, pathologies, etc (see [10, 4, 27], and references therein). Recently, in [22], it has been shown numerically that the linearization of the one dimensional model around a constant state matches in a very suitable manner the nonlinear system itself, even for very realistic test cases.

Since both lumped parameter and one dimensional models are supposed to model the same physiological behavior, one natural question arises : how can two completely different approaches provide comparative answers?

The first direct derivation of a linearized 1D model from axisymmetric Navier-Stokes equations was carried out in [20]. To solve these equations the authors use the electric analog. Namely, they compute an approximate solution using a standard *RLC*-circuit containing a resistor R , an inductor L and a capacitor C . In [6], the authors suggest that “the transmission line can be represented to any desired accuracy by a lumped section” with a reference to the book by Mason [15], based on a sinusoidal steady state analysis. But so far, an analytical and numerical evidence of the latter claim is still missing.

In this article, we give this proof. Precisely, for the particular case of blood flow, we prove that lumped networks can be regarded as first order discretizations of one-dimensional linear systems: More precisely, the solutions of lumped networks converge to that of continuous linear 1D systems when Δx (the length of a single compartment) and Δt (the time step) tend to zero. The convergence is established thanks to Lax-Richtmyer’s theorem, after proving stability using Von-Neumann analysis.

First we establish this result for *RLC* circuits. Starting from the entropy functional associated to the nonlinear one-dimensional hyperbolic system, we derive the energy associated to the linearized one. At the discrete level this energy functional is found to be exactly the instantaneous power dissipated in each compartment of the lumped network. Then the convergence toward a linear hyperbolic system is proven thanks to this energy that “symmetrizes” the scheme.

The standard *RLC* schemes are shown to be stable (and thus convergent) under a “parabolic” CFL condition which severely penalizes the refinement of the spatial grid. In fact, the diagonalization of the scheme shows a preferential direction of waves propagation. Based on this observation, we propose new 0D schemes that use (less restrictive) hyperbolic CFL condition and do not privilege any direction.

The same analysis is then generalised to cover the case of more sophisticated 0D networks accounting for leakage or seepage effects inside large vessels.

Numerical tests show that the difference between the entropy functional and the linear energy is grid independent and almost negligible for realistic blood flow simulations. Moreover, an approximate order of convergence of the solutions computed by lumped models toward the solutions of the continuous linear 1D system is established, confirming the theoretical prediction.

An asymptotic analysis is carried out for small vessels leading to new nonlinear equations. By linearization we obtain a linear heat equation, which could also be obtained as a degenerate case of the linear 1D model previously introduced. The discretization of the heat equation leads to schemes that are suitable to describe an electric circuit containing only a resistor and a capacitor. Again a stability condition guarantees the convergence toward the linear equation.

While for the electric networks the continuity of physical quantities between different elements is ensured by Kirchoff’s laws, the coupling of continuous PDE models needs more careful treatment of interface conditions. The existence of such couplings will be carried on in a future work [17].

An outline of the paper is as follows. With the aim of enhancing readability, we sketch in fig 1 the main items of our road map. Dashed lines and boxes outline the most important contributions brought by this paper.

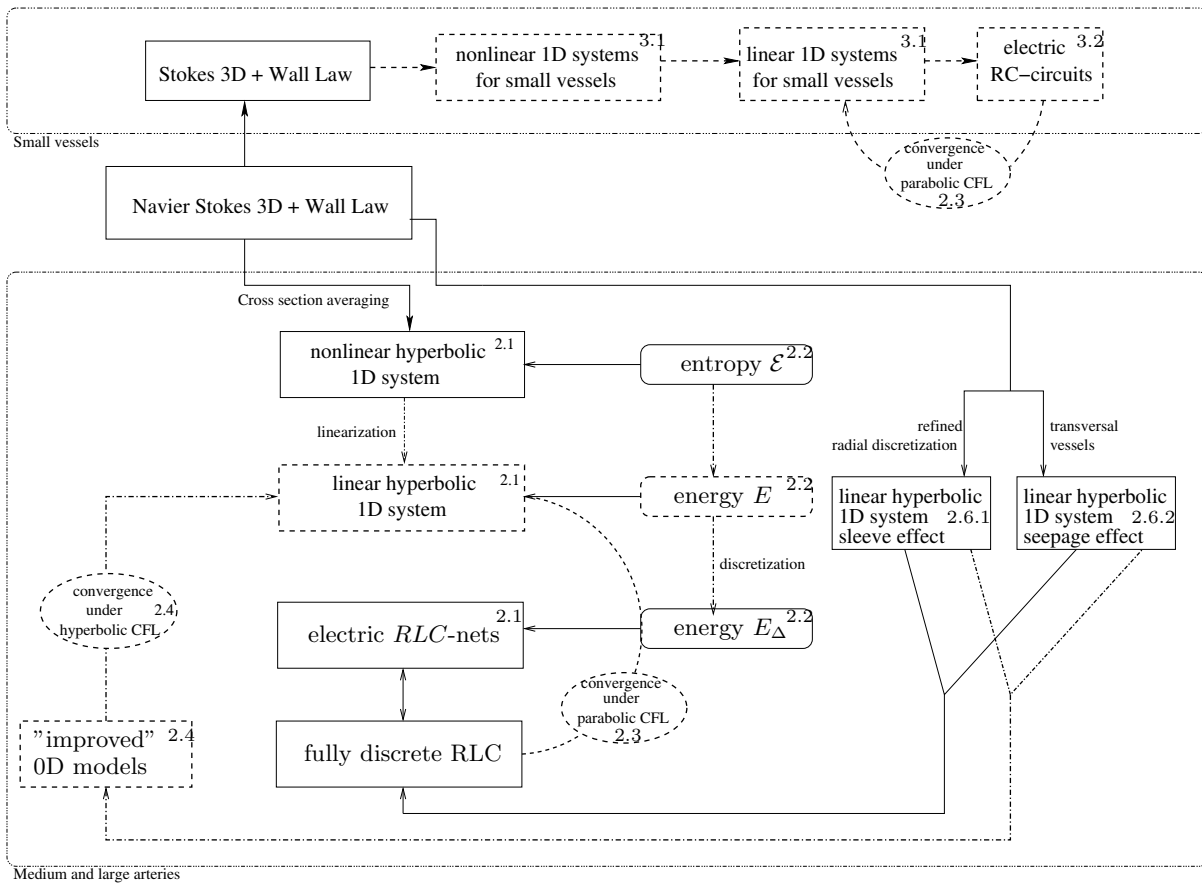


FIGURE 1. A sketch of the hierarchical multiscale models addressed in this paper and the main theoretical results; numbering refers to subsections

In section 2, we study the RLC circuits. At first, in paragraph 2.1, we introduce the RLC network from a novel perspective, by linearizing the cross-sectional 1D approximation of Navier-Stokes equations around a constant state. Then, we use the RLC networks to discretize this linear system. This technique provides exactly

the same definition of the R , L and C constants as already found in [10, 20]. In paragraph 2.2, we introduce the energy estimates allowing us to prove the convergence result. Analyzing the electric scheme, we provide an alternative way of discretizing the RLC system with different upwinded schemes in paragraph 2.4. A numerical evidence is displayed in paragraph 2.5. Then, we perform the same analysis on small vessels leading to the lumped elements associated to the capillary and venous bed (see section 3). Namely, in section 3.1, we derive an 1D incomplete hyperbolic system which is indeed a scalar parabolic equation for blood pressure. Then in section 3.2, by space integration we associate a 0D ODE system which models a RC electric circuit. At this stage we have built a complete hierarchy of nonlinear- linear 1D systems and lumped parameters for blood flow.

2. FROM LINEAR CONSERVATION LAWS TO RLC NETWORKS AND VICE-VERSA

2.1. Deriving the basic \mathcal{L} -circuit equations

A basic description of the RLC network as an approximation of the nonlinear conservation law for blood flow can be found in [10]. The authors use various considerations such as linearization arguments and physical assumptions. Here we introduce the RLC network by following a new approach.

Starting from a simplified version of the Navier-Stokes equations in the axisymmetric form and integrating these equations over each cross-section $A(x, t)$ of the vessel (see [2, 4, 24] and references therein) we obtain the following set of 1D equations, for $0 < x < l$ (l being the vessel length) and all $t > 0$:

$$\begin{cases} \partial_t A + \partial_x Q = 0, \\ \partial_t Q + \partial_x \left(\frac{\alpha Q^2}{A} \right) + \frac{A}{\rho} \partial_x P = -K_r \frac{Q}{A}, \end{cases} \quad (1)$$

where α (the momentum-flux correction coefficient), ρ (the blood density) and K_R (the friction parameter) are supposed to be constant. In particular, K_r is related to the velocity profile assumed in the vessel. If a Poiseuille profile is assumed (which is of course a simplification), $K_r = 8\pi\nu$ (however, see [10] for other possible values). A , P and Q are the unknowns. To close the system we set

$$P(A) = \frac{\beta}{A_0} (\sqrt{A} - \sqrt{A_0}), \quad (2)$$

where A_0 is the section area at rest and the coefficient β supposed constant along the whole vessel, reads $\beta = \frac{\sqrt{\pi} h E}{(1-\sigma^2)}$. The constants E , h and σ are the Young modulus, the wall thickness and the Poisson ratio, respectively. We express the system (1) in (P, Q) variables :

$$\begin{cases} \partial_t P + \partial_A P \partial_x Q = 0, \\ \partial_t Q + \partial_x \left(\alpha \frac{Q^2}{A} \right) + \frac{A}{\rho} \partial_x P = -K_r \frac{Q}{A}. \end{cases} \quad (3)$$

Using the pressure law (2), one has

$$\partial_A P = \frac{\partial P}{\partial A} = \frac{\beta}{2A_0 \sqrt{A}}.$$

The non-conservative form of (3) reads:

$$\partial_t \begin{pmatrix} P \\ Q \end{pmatrix} + \begin{pmatrix} 0 \\ -\alpha u^2 \partial_P A + \frac{A}{\rho} \end{pmatrix} \partial_x \begin{pmatrix} P \\ Q \end{pmatrix} = \begin{pmatrix} 0 & 0 \\ 0 & -\frac{K_r}{A} \end{pmatrix} \begin{pmatrix} P \\ Q \end{pmatrix} \quad (4)$$

where $u = Q/A$ is the mean velocity. Now, by linearizing the system (4) around a constant state $(A, u) = (A_0, 0)$ yields

$$\begin{cases} \partial_t P + \frac{\beta}{2A_0\sqrt{A_0}}\partial_x Q = 0, \\ \partial_t Q + \frac{A_0}{\rho}\partial_x P = -\frac{K_r}{A_0}Q. \end{cases} \quad (5)$$

Remark 2.1. *As pointed out in [22], the choice of this linearization is reasonable as it can reproduce most of the essential features of the blood flow even when modelling the whole systemic tree .*

If we set

$$C' = \frac{2A_0\sqrt{A_0}}{\beta}, \quad L' = \frac{\rho}{A_0}, \quad R' = -\frac{\rho K_r}{A_0^2}, \quad (6)$$

then we can rewrite (5) in a simple linear form

$$\begin{cases} C'\partial_t P + \partial_x Q = 0 \\ L'\partial_t Q + \partial_x P = -R'Q \end{cases} \quad (7)$$

Note that the constants derived here coincide exactly with those of [10]. If we integrate this system in the x direction on the interval $[0, l]$, we have

$$\begin{cases} C\frac{d\hat{P}}{dt} + Q_2 - Q_1 = 0, & t > 0, \\ L\frac{d\hat{Q}}{dt} + P_2 - P_1 = -R\hat{Q}, & t > 0. \end{cases} \quad (8)$$

Here, $\hat{P} = \frac{1}{l}\int_0^l P(x, t)dx$ and $\hat{Q} = \frac{1}{l}\int_0^l Q(x, t)dx$ stand for the mean pressure and flow-rate over the whole compartment, while

$$Q_1(t) = Q(0, t), \quad P_1(t) = P(0, t), \quad Q_2(t) = Q(t, l), \quad P_2(t) = P(t, l),$$

where $x = 0$ is the upstream vessel boundary while $x = l$ is the downstream boundary. The new constants R , L and C read

$$R = R'l, \quad L = L'l, \quad C = C'l.$$

Now assume that some upstream and downstream data are available. For instance suppose that Q_1 and P_2 are given. Then (8) represents a system of two equations and four unknowns. In order to close mathematically problem (8), we make the major assumption that

$$\hat{P} \approx P_1, \quad \hat{Q} \approx Q_2, \quad (9)$$

relating the mean value over the vessel and the pointwise value at the inlet (or outlet) of the vessel. Then,

$$\begin{cases} C\frac{dP_1}{dt} + Q_2 - Q_1 = 0, & t > 0, \\ L\frac{dQ_2}{dt} + P_2 - P_1 = -RQ_2, & t > 0. \end{cases} \quad (10)$$

Remark 2.2. *The waves are smooth and propagate very rapidly inside the cardiovascular system (between 1.5 and 10 m/s), the length of a single tube inside the systemic network can vary between few millimeters up to 10 cm. Thus two pointwise values can be very close for a sufficiently small time delay, justifying why the averaged quantities are themselves close to the pointwise ones. This may explain why assumption (9) should be relevant from the physiological point of view.*

Note that we have identified \hat{P} with the upstream pressure and \hat{Q} with the downstream flow-rate; what follows is coherent with this choice. However, the opposite choice would be acceptable as well, and would lead to a different circuit that we mention later (see Remark 2.3).

In what follows we deal with the issue of “convergence” of 0D-models to 1D-models. To simplify our analysis, we will assume that the 1D system (7) holds for all $x \in \mathbb{R}$, and that it is replaced by an infinite number of elementary circuits like (10) whose length is Δx . More precisely, we connect an infinite number of similar elements

$$\begin{cases} C \frac{dP_i}{dt} = -(Q_{i+1} - Q_i), \\ L \frac{dQ_i}{dt} = -(P_i - P_{i-1}) - RQ_i, \end{cases} \quad (11)$$

where (P_i, Q_i) indicate the pressure and the flow-rate computed at the point $x_i = i\Delta x$ for $i \in \mathbb{Z}$, (note that in the case of finite length, say for $i \in \{1, M\}$ this system would require P_0 to be provided at the inlet (beginning of the network) and Q_{M+1} at the outlet of the network). System (11) can be equivalently regarded as the mathematical description of an electric circuit which is known as \mathcal{L} -circuit (see figure 2.a). In fact, in this hydraulic/electric analogy, pressure and flow rate correspond to the electric voltage and current, the resistance R is related to the blood viscosity, the inductance L to the blood inertia and the capacitance C to the wall compliance.

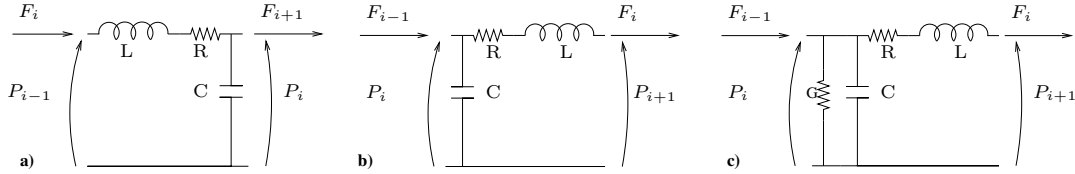


FIGURE 2. The classical \mathcal{L} -circuit (left), the inverse- \mathcal{L} -circuit (center), and the transversal resistor which accounts for seepage effect (right).

In order to establish our convergence result, we shall introduce a specific norm related to the nonlinear entropy function of system (1).

2.2. From nonlinear entropy function to energy dissipated in the \mathcal{L} -circuit

2.2.1. From nonlinear entropy to an energy estimate

One question arises after passing from the nonlinear model (3) to the linearized equations (7) : is there some link between energetic considerations from both sides? The answer represent a new way to connect the entropy function related to instantaneous power dissipated in an electric circuit.

Following [9], an a-priori energy estimate for the nonlinear system (1) can be obtained. Define

$$s(A, u) = \frac{\rho}{2} Au^2 + \Psi \quad (12)$$

where $u = Q/A$ and $\Psi = \Psi(A)$ is given by

$$\Psi(A) = \int_{A_0}^A \psi(\zeta, A_0, \beta) d\zeta. \quad (13)$$

and ψ is a given wall law relating blood pressure and cross-section area. Here we consider a simple algebraic relation:

$$p = \psi(A, A_0, \beta), \quad \text{with } \partial_A \psi > 0 \text{ and } \psi(A_0, A_0, \beta) = 0 \quad (14)$$

for given constants A_0 and β . Then

$$\Psi(A_0) = \Psi'(A_0) = 0, \text{ and } \Psi''(A) > 0, \quad \forall A > 0.$$

Since $\Psi(A)$ is non-negative, so is $s(A, u)$. Thus we can define the averaged total energy of the 1D model by

$$\mathcal{E}(t) = \int_{\mathbb{R}} s(A(x, t), u(x, t)) dx, \quad \forall t > 0. \quad (15)$$

We express Ψ , a function of the cross-section area, as a function of the pressure, namely:

$$\Psi(A) = \int_{A_0}^A \psi(\zeta) d\zeta = \int_{\psi(A_0)}^{\psi(A)} \psi \partial_{\psi} \zeta d\psi = \Upsilon(P), \quad (16)$$

ζ being the cross-section area variable associated with ψ . For the particular case of pressure law given by (2), ζ can be explicitly obtained as a function of ψ as follows

$$\zeta = \left[\frac{A_0}{\beta} \psi + \sqrt{A_0} \right]^2$$

Consequently,

$$\Upsilon(P) = \int_0^P \psi \partial_{\psi} \zeta d\psi = 2 \int_0^P \psi \frac{A_0}{\beta} \left[\frac{A_0}{\beta} \psi + \sqrt{A_0} \right] d\psi = \frac{2}{3} \left(\frac{A_0}{\beta} \right)^2 P^3 + \frac{\sqrt{A_0}^3}{\beta} P^2. \quad (17)$$

The order of magnitude of the pressure inside the arterial tree is approximately $P_a \sim 90 \text{ mmHg} \sim 12000 \text{ dyne/cm}^2$ and the order of magnitude of β is about 10^6 dyne per cm. The cubic term is, in general, 10 to 100 times smaller than the the quadratic one. Thus we can approximate $\Upsilon(P)$ as follows

$$\Upsilon(P) \sim \frac{(\sqrt{A_0})^3}{\beta} P^2 = \frac{C'}{2} P^2,$$

where C' is the constant introduced in (6).

It remains to examine the other term in (12), namely

$$\frac{\rho}{2} A u^2 = \frac{\rho}{2} \frac{Q^2}{A}.$$

Linearizing around the given cross-section area $A = A_0$, we have

$$\frac{\rho}{2} \frac{Q^2}{A} \sim \frac{\rho}{2} \frac{Q^2}{A_0} = \frac{L'}{2} Q^2.$$

Finally, starting from (12), that we rewrite in P, Q variables,

$$s(A, Q) = \frac{\rho}{2} \left(\frac{Q}{\frac{A_0}{\beta} P + \sqrt{A_0}} \right)^2 + \frac{2}{3} \left(\frac{A_0}{\beta} \right)^2 P^3 + \frac{\sqrt{A_0}^3}{\beta} P^2 \equiv e(P, Q), \quad (18)$$

we obtain the following “linearized energy” functional

$$e_{\text{lin}}(P, Q) = \left(\frac{C'}{2} P^2 + \frac{L'}{2} Q^2 \right) \quad (19)$$

that suggests the introduction of the following norm

$$\begin{aligned} E(P, Q)(t) &= \left(\int_{\mathbb{R}} e_{\text{lin}}(P(x, t), Q(x, t)) dx \right)^{\frac{1}{2}} = \left(\int_{\mathbb{R}} \left(\frac{C'}{2} P^2 + \frac{L'}{2} Q^2 \right) (x, t) dx \right)^{\frac{1}{2}} \\ &= \left(\frac{C'}{2} \|P\|_{L^2(\mathbb{R})}^2 + \frac{L'}{2} \|Q\|_{L^2(\mathbb{R})}^2 \right)^{\frac{1}{2}}, \end{aligned} \quad (20)$$

equivalent to the $L^2(\mathbb{R})$ norm. Multiplying the first equation of (7) by P , the second by Q , summing up the two equations and integrating over \mathbb{R} , we get:

Lemma 2.1. *The solutions of system (7) are stable w.r. to norm E defined in (20); precisely*

$$\frac{d}{dt} E(P, Q)^2 = -R \int_{\mathbb{R}} Q^2(x, t) dx \leq 0, \quad \forall t \geq 0. \quad (21)$$

This proposition provides energy estimates for the linearized system as the nonlinear entropy function guarantees the stability for solutions of the nonlinear system (1) (see [9]).

2.2.2. From dissipated power in the \mathcal{L} -circuit to a discrete energy estimate

If we compute the instantaneous power dissipated in both branches of a single \mathcal{L} -circuit described by (11), we have [7] :

$$\Pi_i = Q_{C,i} P_{C,i} + Q_{RL,i} P_{RL,i}, \quad (22)$$

where $(P_{C,i}, Q_{C,i})$ are the values of pressure and flow-rate in the capacitor part, while $(P_{RL,i}, Q_{RL,i})$ are those crossing the resistance R and the inductance L . The pressure in the latter branch reads

$$P_{RL,i} = P_{i-1} - P_i,$$

while the pressure inside the capacitor is simply P_i . For the flow rate, by definition of a capacitor, we have

$$Q_{C,i} = C \frac{d}{dt} P_i.$$

Summing (22) over i , and using the first equation of (11), one can write

$$\sum_i \Pi_i = \sum_i -(Q_{i+1} - Q_i) P_i + Q_i (P_{i-1} - P_i) = 0$$

which is the consequence of Kirchoff's laws. Re-expressing the latter equation one can write

$$\sum_i \Pi_i = \frac{C}{2} \sum_i \frac{d}{dt} P_i^2 + \frac{L}{2} \sum_i \frac{d}{dt} Q_i^2 + \sum_i R Q_i^2 = 0$$

Thus, we recover a stability estimate for the solutions of (11) in a discrete version of the norm (20), namely we can claim

Lemma 2.2. *Let us introduce the discrete energy*

$$E_{\Delta}(P_{\Delta}, Q_{\Delta}) = \left(\frac{C'}{2} \sum_i \Delta x P_i^2 + \frac{L'}{2} \sum_i \Delta x Q_i^2 \right)^{\frac{1}{2}} = \left(\frac{C'}{2} \|P_{\Delta}\|_{l^2(\mathbb{R})}^2 + \frac{L'}{2} \|Q_{\Delta}\|_{l^2(\mathbb{R})}^2 \right)^{\frac{1}{2}} \quad (23)$$

For the solution (P_Δ, Q_Δ) of an infinite network of \mathcal{L} -circuits described by the semi-discrete scheme (11), the following discrete energy estimates holds

$$\frac{d}{dt}(E_\Delta(P_\Delta, Q_\Delta))^2 = -R'\|Q_\Delta\|_{L^2(\mathbb{R})}^2 \leq 0. \quad (24)$$

In section 2.1 we show how to build a hierarchy of models passing from 1D-nonlinear equations to the linear 1D system and ending with the 0D discretization. So it is possible to derive the corresponding hierarchy of energy estimates associated to each model. In what follows we use the previous norms to ensure the convergence of fully discrete schemes toward the solutions of the continuous system (7).

2.3. Convergence of (11) to (7)

If we turn back to the adimensionalized constants R' , L' and C' , we can write (11) as

$$\begin{cases} C' \frac{dP_i}{dt} = -\frac{1}{\Delta x}(Q_{i+1} - Q_i) \\ L' \frac{dQ_i}{dt} = -R'Q_i - \frac{1}{\Delta x}(P_i - P_{i-1}). \end{cases} \quad (25)$$

where Δx denotes now the (constant) length of the i -th element of the network. If we regard Q_i as being the pointwise value at $x = x_i$ of the flow-rate function $Q(x, t)$ (that we assume regular enough), and the same assumption is made for P_i , then

$$\begin{cases} Q(x_{i+1}, t) = Q(x_i, t) + \Delta x \partial_x Q(x_i, t) + \frac{\Delta x^2}{2} \partial_{xx} Q(x_i, t) + O(\Delta x^3), \\ P(x_{i-1}, t) = P(x_i, t) - \Delta x \partial_x P(x_i, t) + \frac{\Delta x^2}{2} \partial_{xx} P(x_i, t) + O(\Delta x^3), \end{cases}$$

we draw that (25) can be regarded as a first order approximation in space of system (7). In this section, we prove that the scheme provided by the semi discrete system (25) is stable. Then, a linear scheme being stable and consistent, it is also convergent owing to the Lax-Richtmyer equivalence theorem (by Von Neumann analysis) [29].

We discretize the system (25) in time using the first order forward Euler scheme,

$$\begin{cases} P_i^{n+1} = P_i^n - \frac{\lambda}{C'}(Q_{i+1}^n - Q_i^n), \\ Q_i^{n+1} = (1 - \frac{R'}{L'}\Delta t)Q_i^n - \frac{\lambda}{L'}(P_i^n - P_{i-1}^n), \end{cases} \quad (26)$$

where P_i^n is an approximation of $P(x_i, t^n = n\Delta t)$ (and Q_i^n of $Q(x_i, t^n = n\Delta t)$), Δt being the time step, and $\lambda = \frac{\Delta t}{\Delta x}$ is the Courant number.

Theorem 2.1. *The scheme (26) is unstable in the $L^2(\mathbb{R})$ norm under any hyperbolic CFL condition, i.e. if $\lambda \leq k$ for any choice of k independent of Δt and Δx . However, under the “parabolic CFL condition”*

$$\Delta t < \min\left(\frac{R'C'\Delta x^2}{2}, \frac{L'}{R'}\right) \quad (27)$$

the scheme is stable for the E_Δ norm defined by (24). Moreover it provides solutions converging to the solution of system (7) w.r. to the $L^2(\mathbb{R})$ or E norms.

PROOF. Using the inverse Fourier transform formula we have

$$\begin{cases} P_m^n = \frac{1}{\sqrt{2\pi}} \int_{-\frac{\pi}{\Delta x}}^{\frac{\pi}{\Delta x}} e^{im\Delta x\xi} \hat{P}^n(\xi) d\xi, \\ Q_m^n = \frac{1}{\sqrt{2\pi}} \int_{-\frac{\pi}{\Delta x}}^{\frac{\pi}{\Delta x}} e^{im\Delta x\xi} \hat{Q}^n(\xi) d\xi, \end{cases} \quad (28)$$

substituting this in (26) for $Q_{m+1}^n, Q_m^n, P_m^n, P_{m-1}^n$, we obtain

$$\begin{cases} P_m^{n+1} = \frac{1}{\sqrt{2\pi}} \int_{-\frac{\pi}{\Delta x}}^{\frac{\pi}{\Delta x}} e^{im\Delta x\xi} \left[\hat{P}^n(\xi) - \frac{\lambda}{C'} (e^{i\Delta x\xi} - 1) \hat{Q}^n(\xi) \right] d\xi \\ Q_m^{n+1} = \frac{1}{\sqrt{2\pi}} \int_{-\frac{\pi}{\Delta x}}^{\frac{\pi}{\Delta x}} e^{im\Delta x\xi} \left[\left(1 - \frac{R'}{L'} \Delta t\right) \hat{Q}^n - \frac{\lambda}{L'} (1 - e^{-i\Delta x\xi}) \hat{P}^n(\xi) \right] d\xi, \end{cases} \quad (29)$$

The Fourier transform being unique [29], we identify (29) and the formula (28) taken at the next time step t^{n+1} , to write:

$$\begin{pmatrix} \hat{P}^{n+1} \\ \hat{Q}^{n+1} \end{pmatrix} = \begin{pmatrix} 1 & \frac{\lambda}{C'} z \\ -\frac{\lambda}{L'} z & 1 - \alpha \end{pmatrix} \begin{pmatrix} \hat{P}^n \\ \hat{Q}^n \end{pmatrix} \quad (30)$$

where we have set $\alpha = \frac{R'}{L'} \Delta t$ and $z = 1 - e^{-i\Delta x\xi}$. We call \mathcal{A} the amplification matrix in equation (30), and is function of the frequency ξ and the constants R', L', C' and $\Delta t, \Delta x$.

In a first time, we estimate $\rho(\mathcal{A})$, the spectral radius of \mathcal{A} in order to obtain a necessary condition of convergence.

Study of $\rho(\mathcal{A})$. The eigenvalues of \mathcal{A} can be found by inspecting the roots of the characteristic polynomial

$$\det(\mathcal{A} - \beta I) = \beta^2 - (2 - \alpha)\beta + (1 - \alpha + \lambda^2 \frac{|z|^2}{L'C'}), \quad (31)$$

the associated discriminant is

$$\Delta(\xi) = \alpha^2 - 4\lambda^2 \frac{|z|^2}{L'C'}, \quad \text{with } |z|^2 = 4 \sin^2 \left(\frac{\Delta x \xi}{2} \right). \quad (32)$$

The sign of $\Delta(\xi)$ as function of ξ

At first, we can remark that $\Delta(\xi)$ is a monotone in $[0, \frac{\pi}{\Delta x}]$. We notice that $\Delta(0) = \alpha^2 > 0$. Then if $\Delta x < \frac{2}{R'} \sqrt{\frac{L'}{C'}}$, one guarantees that $\Delta(\frac{\pi}{\Delta x}) < 0$. This yields the existence of a unique root of Δ on $[0, \frac{\pi}{\Delta x}]$ which is

$$\xi_0 = \frac{2}{\Delta x} \arcsin \left(\frac{R'}{4} \sqrt{\frac{C'}{L'}} \Delta x \right)$$

For y small enough, $\arcsin(y)$ behaves like $y + \frac{1}{6}y^3 + O(y^5)$ yielding

$$\xi_0 = \frac{R'}{2} \sqrt{\frac{C'}{L'}} + \frac{R'^3 \Delta x^2}{3 \cdot 4^3} \left(\frac{C'}{L'} \right)^{\frac{3}{2}} + O(\Delta x^4). \quad (33)$$

This means that ξ_0 belong to a small neighborhood of $\frac{R'}{2} \sqrt{\frac{C'}{L'}}$ whose width depends on Δx .

As $\Delta(\xi)$ is monotone there are two subsets of $[-\frac{\pi}{\Delta x}, \frac{\pi}{\Delta x}]$, where its sign is constant. We call

$$V_{\text{ext}}(\xi_0) = \left[-\frac{\pi}{\Delta x}, -\xi_0 \right] \cup \left[\xi_0, \frac{\pi}{\Delta x} \right],$$

the subset where $\Delta(\xi)$ is negative, while in $V_{\text{int}}(\xi_0) =]-\xi_0, \xi_0[$, $\Delta(\xi)$ is positive.

The case $\xi \in V_{\text{ext}}(\xi_0)$

As $\Delta(\xi) < 0$, in this region the roots of (31) are complex

$$|\beta_{\pm}|^2 = 1 - \alpha + \frac{\lambda^2 |z|^2}{L'C'}.$$

1) Hyperbolic CFL condition: λ is constant

If we take Δx small enough so that $\frac{\pi}{2\Delta x}$ belongs to the interior of $V_{\text{ext}}(\xi_0)$, one can write

$$\forall \xi \in \left] \frac{\pi}{2\Delta x} + \frac{C'R'}{2\lambda}, \frac{\pi}{\Delta x} \right], \quad \sin^2 \left(\frac{\Delta x \xi}{2} \right) \geq \frac{1}{2} + \frac{L'C'}{4\lambda^2} \alpha. \quad (34)$$

Note that $\frac{C'R'}{2\lambda}$ is a constant, implying that there exists Δx small enough such that $\frac{\pi}{2\Delta x} + \frac{C'R'}{2\lambda} < \frac{\pi}{\Delta x}$. Then (34) provides the lower bound for the eigenvalues:

$$1 + \frac{2\lambda^2}{L'C'} < |\beta_{\pm}(\xi)| = \rho(\mathcal{A}).$$

2) “Parabolic” CFL condition: $\Delta t < (R'C'\Delta x^2/4)$

On the contrary, for this type of condition we have that

$$|\beta_{\pm}(\xi)| \leq 1 - \alpha + \frac{4\lambda^2}{L'C'} < 1, \quad \forall \xi \in V_{\text{ext}}(\xi_0)$$

For the rest of the frequency spectrum, $\rho(\mathcal{A})$ is less or equal to one, for Δt small enough.

The sufficient condition. Here we show the sufficient condition of stability under a “parabolic” CFL condition. The Parseval relation gives :

$$\|P\|_{l^2}^2 = \Delta x \sum_i P_i^2 = \|\hat{P}\|_{L^2(-\frac{\pi}{\Delta x}, \frac{\pi}{\Delta x})}^2 = \int_{-\frac{\pi}{\Delta x}}^{\frac{\pi}{\Delta x}} |\hat{P}|^2 d\xi,$$

thus we can write

$$[E_{\Delta}(P, Q)]^2 = \frac{C'}{2} \|P\|_{l^2}^2 + \frac{L'}{2} \|Q\|_{l^2}^2 = \frac{C'}{2} \|\hat{P}\|_{L^2(-\frac{\pi}{\Delta x}, \frac{\pi}{\Delta x})}^2 + \frac{L'}{2} \|\hat{Q}\|_{L^2(-\frac{\pi}{\Delta x}, \frac{\pi}{\Delta x})}^2$$

We set $D = \text{diag}(\sqrt{\frac{C'}{2}}, \sqrt{\frac{L'}{2}})$, $X = \begin{pmatrix} \hat{P} \\ \hat{Q} \end{pmatrix}$, and we define the 2-norm of X in \mathbb{C}^2 by $\|X\|_2 = \sqrt{|\hat{P}|^2 + |\hat{Q}|^2}$, then the previous energy term becomes

$$[E_{\Delta}(P, Q)]^2 = \int_{-\frac{\pi}{\Delta x}}^{\frac{\pi}{\Delta x}} \|DX(\xi)\|_2^2 d\xi = \int_{-\frac{\pi}{\Delta x}}^{\frac{\pi}{\Delta x}} \|X(\xi)\|_D^2 d\xi$$

where $\|X\|_D = \|DX\|_2$. Applying matrix D to (30) leads for a fixed ξ to

$$DX^{n+1}(\xi) = DA(\xi)D^{-1}DX^n(\xi), \quad \forall \xi \in \left] \frac{-\pi}{\Delta x}; \frac{\pi}{\Delta x} \right[$$

which gives the following estimate

$$\|X^{n+1}(\xi)\|_D^2 \leq \|D\mathcal{A}(\xi)D^{-1}\|_2^2 \|X^n(\xi)\|_D^2, \quad \forall \xi \in \left] \frac{-\pi}{\Delta x}; \frac{\pi}{\Delta x} \right[.$$

The quantity $\|D\mathcal{A}D^{-1}\|_2^2$ can be explicitly computed as

$$\|D\mathcal{A}D^{-1}\|_2^2 = \rho((D\mathcal{A}D^{-1})^* D\mathcal{A}D^{-1}).$$

The entries of the symmetric matrix $\mathcal{N} = (D\mathcal{A}D^{-1})^* D\mathcal{A}D^{-1}$ are easy to obtain, and read

$$\mathcal{N} = \begin{pmatrix} 1 + \frac{\lambda^2|z|^2}{L'C'} & -\alpha \frac{\lambda\bar{z}}{\sqrt{L'C'}} \\ -\alpha \frac{\lambda z}{\sqrt{L'C'}} & \frac{\lambda^2|z|^2}{L'C'} + (1-\alpha)^2 \end{pmatrix}.$$

Its eigenvalues are

$$\beta_{\pm} = \frac{2 + 2a + \Gamma \pm \sqrt{\Gamma^2 + 4a\alpha}}{2}$$

where $a = \frac{\lambda^2|z|^2}{L'C'}$ and $\Gamma = \alpha(\alpha - 2)$. At this point, if we suppose that $\alpha < 1$ and that $\frac{4\lambda^2}{L'C'} < \alpha$, then for every ξ , $a < \alpha$ and

$$\beta_{\pm} < \left(1 + \frac{\sqrt{3}}{2}\alpha\right)^2.$$

Finally, this gives the energy estimate :

$$\begin{aligned} E_{\Delta}(P^{n+1}, Q^{n+1}) &\leq (1 + 2\sqrt{3}\alpha)E_{\Delta}(P^n, Q^n) \leq (1 + 2\sqrt{3}\alpha)^n E_{\Delta}(P^0, Q^0) \\ &\leq e^{\frac{\sqrt{3}R'}{2L'}(n+1)\Delta t} E_{\Delta}(P^0, Q^0) \leq e^{\frac{\sqrt{3}R'}{2L'}(T+1)} E_{\Delta}(P^0, Q^0), \end{aligned} \quad (35)$$

where the bound is uniform in Δt and Δx .

Instability under the hyperbolic CFL condition. To prove that the solution blows up in finite time for such a CFL condition, we take a particular solution. Let $v(\xi)$ be an eigenvector of \mathcal{A} associated to the biggest eigenvalue β_+ . Then

$$v(\xi) = \begin{pmatrix} \alpha + \sqrt{\Delta} \\ -\frac{2\lambda z}{L'} \end{pmatrix}, \quad \beta_+ = \frac{2 - \alpha + \sqrt{\Delta}}{2}, \quad \Delta = \alpha^2 - 4\frac{\lambda^2|z|^2}{L'C'}.$$

We can provide a lower bound for $v(\xi)$ in the 2-norm as follows

$$\|v(\xi)\|_2^2 = \alpha^2 + |\Delta| + 4\frac{\lambda^2|z|^2}{(L')^2} \geq 4\frac{\lambda^2|z|^2}{(L')^2}, \quad \forall \xi \in V_{\text{ext}}(\xi_0).$$

We call $\gamma = \frac{C'R'}{2\lambda}$, and we set $I(\xi) = \mathbb{I}_{\left[\frac{\pi}{2\Delta x} + \gamma, \frac{\pi}{\Delta x}\right]}(\xi)$, the characteristic function of $\left[\frac{\pi}{2\Delta x} + \gamma, \frac{\pi}{\Delta x}\right]$. We set the Fourier transform of the initial condition to be

$$X^0(\xi) = \left(\frac{L'}{\lambda\sqrt{2}} \sqrt{\frac{\Delta x}{\frac{\pi}{2} - \gamma\Delta x}} \right) I(\xi)v(\xi), \quad \forall \xi \in \left[-\frac{\pi}{\Delta x}, \frac{\pi}{\Delta x}\right].$$

For any fixed Δx , this function belongs to $L^2\left(-\frac{\pi}{\Delta x}, \frac{\pi}{\Delta x}\right)$. Applying (30) to this particular initial data gives the explicit solution as

$$X^n = \beta_+^n X^0.$$

Then, the following estimate holds

$$\begin{aligned} \|X^n\|_{L^2(\mathbb{R})}^2 &= \int_{-\frac{\pi}{\Delta x}}^{\frac{\pi}{\Delta x}} |\beta_+|^{2n} \|X^0\|_2^2 d\xi = \frac{(L')^2 \Delta x}{2\lambda^2 (\frac{\pi}{2} - \gamma \Delta x)} \int_{\frac{\pi}{2\Delta x} + \gamma}^{\frac{\pi}{\Delta x}} |\beta_+|^{2n} \|v(\xi)\|_2^2 d\xi \\ &\geq \left(1 + \frac{2\lambda^2}{L'C'}\right)^{2n} \end{aligned}$$

For a hyperbolic CFL condition, the Courant number λ is a fixed constant, and thanks to the previous inequality there is no possible bound for X^n in $L^2(-\frac{\pi}{\Delta x}, \frac{\pi}{\Delta x})$. \square

Remark 2.3. *Another configuration of lumped circuit, called the inverse- \mathcal{L} network, is driven by the following system of equations*

$$\begin{cases} C' \frac{dP_i}{dt} = -\frac{1}{\Delta x} (Q_i - Q_{i-1}) \\ L' \frac{dQ_i}{dt} = -R' Q_i - \frac{1}{\Delta x} (P_{i+1} - P_i). \end{cases} \quad (36)$$

This is the symmetric form of the system (25), and is sketched by the electric network on figure 2.b. For this network, the Von Neumann analysis follows the same lines until one obtains the same discriminant (32) that guides the amplification matrix. Then it is clear that both networks can be regarded as approximations of the system (7).

2.4. New 0D schemes for blood flow

2.4.1. The characteristic variables and the related diagonal system

Through the change of variables

$$\begin{pmatrix} w \\ z \end{pmatrix} = \frac{1}{2} \begin{pmatrix} 1 & \sqrt{\frac{L'}{C'}} \\ 1 & -\sqrt{\frac{L'}{C'}} \end{pmatrix} \begin{pmatrix} P \\ Q \end{pmatrix},$$

the system (7) becomes

$$\begin{cases} \partial_t w + \frac{1}{\sqrt{C'L'}} \partial_x w = -\frac{R'}{2L'} (w - z) \\ \partial_t z - \frac{1}{\sqrt{C'L'}} \partial_x z = \frac{R'}{2L'} (w - z), \end{cases} \quad (37)$$

where (w, z) are called the characteristic variables. This system is completely decoupled in the differential part, the two equations being coupled only by the source term.

The scheme (26) rewritten for the characteristic variables, becomes

$$\begin{cases} w_i^{n+1} = (1 - \frac{R'}{2L'} \Delta t) w_i^n - \frac{\lambda}{2\sqrt{L'C'}} [w_{i+1}^n - w_{i-1}^n] + \frac{\lambda}{\sqrt{L'C'}} \left\{ \frac{z_{i+1}^n - 2z_i^n + z_{i-1}^n}{2} \right\} + \frac{R'}{2L'} \Delta t z_i^n, \\ z_i^{n+1} = (1 - \frac{R'}{2L'} \Delta t) z_i^n + \frac{\lambda}{2\sqrt{L'C'}} [z_{i+1}^n - z_{i-1}^n] - \frac{\lambda}{\sqrt{L'C'}} \left\{ \frac{w_{i+1}^n - 2w_i^n + w_{i-1}^n}{2} \right\} + \frac{R'}{2L'} \Delta t w_i^n, \end{cases} \quad (38)$$

This corresponds to having discretized the characteristic system (37) by centered differences with the addition of two terms, one dissipative for the first equation, the other antidissipative for the latter one. This asymmetry indicates that the \mathcal{L} -circuit prioritizes backward waves and damps the amplitude of the forward ones. The centered differences are unstable under hyperbolic CFL conditions which might explain why we need a parabolic

CFL condition to stabilize the numerical solutions. In the same way for an explicit discretization of (36), one has

$$\begin{cases} w_i^{n+1} = (1 - \frac{R'}{2L'}\Delta t)w_i^n - \frac{\lambda}{2\sqrt{L'C'}}[w_{i+1}^n - w_{i-1}^n] - \frac{\lambda}{\sqrt{L'C'}} \left\{ \frac{z_{i+1}^n - 2z_i^n + z_{i-1}^n}{2} \right\} + \frac{R'}{2L'}\Delta t z_i^n \\ z_i^{n+1} = (1 - \frac{R'}{2L'}\Delta t)z_i^n + \frac{\lambda}{2\sqrt{L'C'}}[z_{i+1}^n - z_{i-1}^n] + \frac{\lambda}{\sqrt{L'C'}} \left\{ \frac{w_{i+1}^n - 2w_i^n + w_{i-1}^n}{2} \right\} + \frac{R'}{2L'}\Delta t w_i^n \end{cases} \quad (39)$$

which is the complementary version of (38). Here again we see the opposite sign on the second order terms.

2.4.2. Correctly upwinded 0D schemes

Thanks to the previous arguments, we can list the major drawbacks of the standard electric circuits : expensive CFL, asymmetric wave propagation, no strict decrease of energy in the E_Δ norm (only a time exponential bound is available from (35)). To remove them, we propose here new schemes inspired by convenient hyperbolic discretizations of system (7).

- First order discretization in space

A space discretization of system (7) by first order upwind schemes yields

$$\begin{cases} C\partial_t P_i = -\frac{1}{2}[Q_{i+1} - Q_{i-1}] + \frac{1}{2}\sqrt{\frac{C}{L}}(P_{i+1} - 2P_i + P_{i-1}) \\ L\partial_t Q_i = -\frac{1}{2}[P_{i+1} - P_{i-1}] + \frac{1}{2}\sqrt{\frac{L}{C}}(Q_{i+1} - 2Q_i + Q_{i-1}) - RQ_i \end{cases} \quad (40)$$

Its forward Euler time discretization gives the well-known Lax-Friedrichs' scheme. This scheme is strictly stable in the E_Δ norm, namely it's easy to prove the following result

Corollary 2.1. *Under the CFL condition :*

$$\Delta t \leq \sqrt{L'C'}\Delta x = \sqrt{LC},$$

the solution given by forward Euler time discretization of (40) satisfies the following energy estimate

$$E_\Delta(P^{n+1}, Q^{n+1}) \leq E_\Delta(P^n, Q^n)$$

The proof is straightforward, indeed in the characteristic variables the scheme reduces to the first order upwind scheme in both directions that can be set in a convex form. This ensures the decrease of E_Δ in time.

- A second order discretization in space can be used as well

For regular solutions it could be the Lax-Wendroff scheme:

$$\begin{cases} P_i^{n+1} = P_i^n - \frac{\Delta t}{2C}[Q_{i+1}^n - Q_{i-1}^n] + \frac{\Delta t^2}{2LC}(P_{i+1}^n - 2P_i^n + P_{i-1}^n) \\ Q_i^{n+1} = (1 - \alpha)Q_i^n - \frac{\Delta t}{2L}[P_{i+1}^n - P_{i-1}^n] + \frac{\Delta t^2}{2LC}(Q_{i+1}^n - 2Q_i^n + Q_{i-1}^n). \end{cases} \quad (41)$$

For less regular ones, a MUSCL scheme can be set up

$$\begin{cases} Q_i^{n+1} = (1 - \alpha)Q_i^n - \frac{\Delta t}{2L} [P_{i+1}^n - P_{i-1}^n] + \frac{\Delta t}{2\sqrt{LC}}(Q_{i+1}^n - 2Q_i^n + Q_{i-1}^n) \\ \quad - \frac{1}{2}\left(1 - \frac{\Delta t}{\sqrt{LC}}\right)\frac{\Delta t}{\sqrt{LC}} * \sqrt{\frac{C}{L}} * (\sigma_{1,i}^n - \sigma_{1,i-1}^n - \sigma_{2,i+1}^n + \sigma_{2,i}^n), \\ P_i^{n+1} = P_i^n - \frac{\lambda}{2C'} [Q_{i+1}^n - Q_{i-1}^n] + \frac{\Delta t}{2\sqrt{LC}}(P_{i+1}^n - 2P_i^n + P_{i-1}^n) \\ \quad - \frac{1}{2}\left(1 - \frac{\Delta t}{\sqrt{LC}}\right)\frac{\Delta t}{\sqrt{LC}} * (\sigma_{1,i}^n - \sigma_{1,i-1}^n + \sigma_{2,i+1}^n - \sigma_{2,i}^n). \end{cases} \quad (42)$$

here $\alpha = \Delta t \frac{R}{L}$, and $\sigma_{1,i}^n = \min \text{mod}(w_{i+1}^n - w_i^n, w_i^n - w_{i-1}^n)$, and $\sigma_{2,i}^n = \min \text{mod}(z_{i+1}^n - z_i^n, z_i^n - z_{i-1}^n)$ are the slope limiters ensuring the $L^1 \cap L^\infty$ stability of the scheme (see [12] for more details).

The major difference when discretizing system (7) with some upwind scheme relies on the way the variables are exchanged with neighbor elements: while the \mathcal{L} network takes the pressure P_{i-1} from the left neighbor cell and the flow rate Q_{i+1} from the right one (see (11)), upwind schemes need both physical quantities on each side.

2.5. Numerical assessment

In this section, we perform a numerical simulation in order to check the above theoretical results. Using scheme (11), we compute the pressure P_{0D} , the flow rate Q_{0D} inside a vessel of fixed length (60 cm), for different grid-size Δx .

For each Δx , we display the difference between the entropy functional e from (18) and the linear energy e_{lin} given in (19). Precisely, for each pair of solutions (P_{0D}, Q_{0D}) we compute

$$R_\Delta = \frac{\sum_{i,n} |e(P_{0D,i}^n, Q_{0D,i}^n) - e_{\text{lin}}(P_{0D,i}^n, Q_{0D,i}^n)|}{\sum_{i,n} e(P_{0D,i}^n, Q_{0D,i}^n)}.$$

We show in table 1, that this quantity is grid independent (which is expected because it is the discrete version of continuous functionals) and that the error is of only 4% approximatively. Then, we compare (P_{0D}, Q_{0D}) to the numerical solution of (7) computed using the second order Lax-Wendroff scheme on a very refined grid (1000 grid-cells). In the third row of table 1, using again the E_Δ norm, we compute

$$\begin{aligned} e_{\Delta x} &= \left(\sum_n E_\Delta(P_{0D}^n - P_{ex}(\cdot, t^n), Q_{0D}^n - Q_{ex}(\cdot, t^n)) \right)^{\frac{1}{2}} \\ &= \left(\Delta t \Delta x \sum_{n,i} e_{\text{lin}}(P_{0D,i}^n - P_{ex}(x_i, t^n), Q_{0D,i}^n - Q_{ex}(x_i, t^n)) \right)^{\frac{1}{2}}. \end{aligned}$$

Then, the approximate order of convergence α_{app} is computed thanks to the standard formula [19] :

$$\alpha_{\text{app}} = \frac{\log(e_{\Delta x_1}/e_{\Delta x_2})}{\log(\Delta x_1/\Delta x_2)}.$$

and its value (see forth row in table 1) corresponds actually to the first order exhibited when using the Taylor expansion. In figure 4, we plot: the solution of the non-linear system (1) obtained using a second order Taylor-Galerkin scheme [9], the linear solution used as reference in the previous table, and the solution (P_{0D}, Q_{0D}) obtained for a grid size $\Delta x = 1.2\text{cm}$. We plot these solutions at four different locations in space ($x = 0, x = 20$,

Δx cm	R_Δ	$e_{\Delta x}$	α
6.0000	0.0489	414.2032	1.0969
1.2000	0.0416	70.8780	1.0998
0.6000	0.0409	33.0700	1.1840
0.3000	0.0405	14.5550	1.5399
0.1200	0.0403	3.5500	–

TABLE 1. Error between the two energy functionals, 0D solution against 1D linear solution and order of convergence

$x = 40$ and $x = 60$ cm). The time is given in seconds on the x-axis during two cycles. The pressure is imposed at the left boundary (see left upper corner of figure 3), and the flow-rate is given at the right outflow (right down corner in figure 3)). We can observe that the difference between the solution of the linear system (7) and the 0D solution is negligible, while the differences are more important with the solution of the nonlinear system (1), however the non-linearity plays a role for high frequencies only. For the solution of (1), we plot the curves of E_Δ and \mathcal{E}_Δ (the latter is the discrete version of \mathcal{E} introduced in (15)), in time over two cycles again. Differences are negligible, but they appear for higher values of pressure where the cubic term starts to account. We remark that entropy and energy do not decrease simply because the solutions is computed on a bounded interval with imposed boundary conditions at both ends of the interval.

We consider a vessel whose length is 60 cm, its radius 0.5 cm, and its thickness 0.1 cm. The blood viscosity is equal to $0.035 \text{ cm}^2/\text{s}$, its density is set to 1 g/cm^3 , the Young modulus is set to $3 \cdot 10^6 \text{ dyne/cm}^2$, while the momentum-flux correction coefficient α is set to one (these data are taken from [10, p 1.24]).

2.6. RLC Systems accounting for more particular effects

2.6.1. Blood seepage

Blood seepage (due e.g. to some small branches that we do not want to model) can be accounted in the original RLC \mathcal{L} and inverse- \mathcal{L} circuits by adding some transversal resistance G governing the amount of seepage (see [14, 10]). In [30], the coefficient G is defined as a function of the length of the section as

$$G = \frac{G'}{\Delta x}.$$

For the exact definition of G' with respect to the physical constants of the vessel see [14]. The corresponding scheme related to this network (see fig 2.c), is obtained by modifying the system (11) as follows :

$$\begin{cases} C' \frac{dP_i}{dt} = -\frac{1}{\Delta x}(Q_{i+1} - Q_i) - \frac{P_i}{G'}, \\ L' \frac{dQ_i}{dt} = -R'Q_i - \frac{1}{\Delta x}(P_i - P_{i-1}), \end{cases} \quad (43)$$

Applying again Lax-Richtmyer's theorem we can claim

Corollary 2.2. *Under the following parabolic CFL condition*

$$\Delta t \leq \min \left(\left(\frac{C'R' + \frac{L'}{G'}}{4 + \frac{R'}{G'}} \right) \Delta x^2, \frac{L'}{R'}, C'G' \right)$$

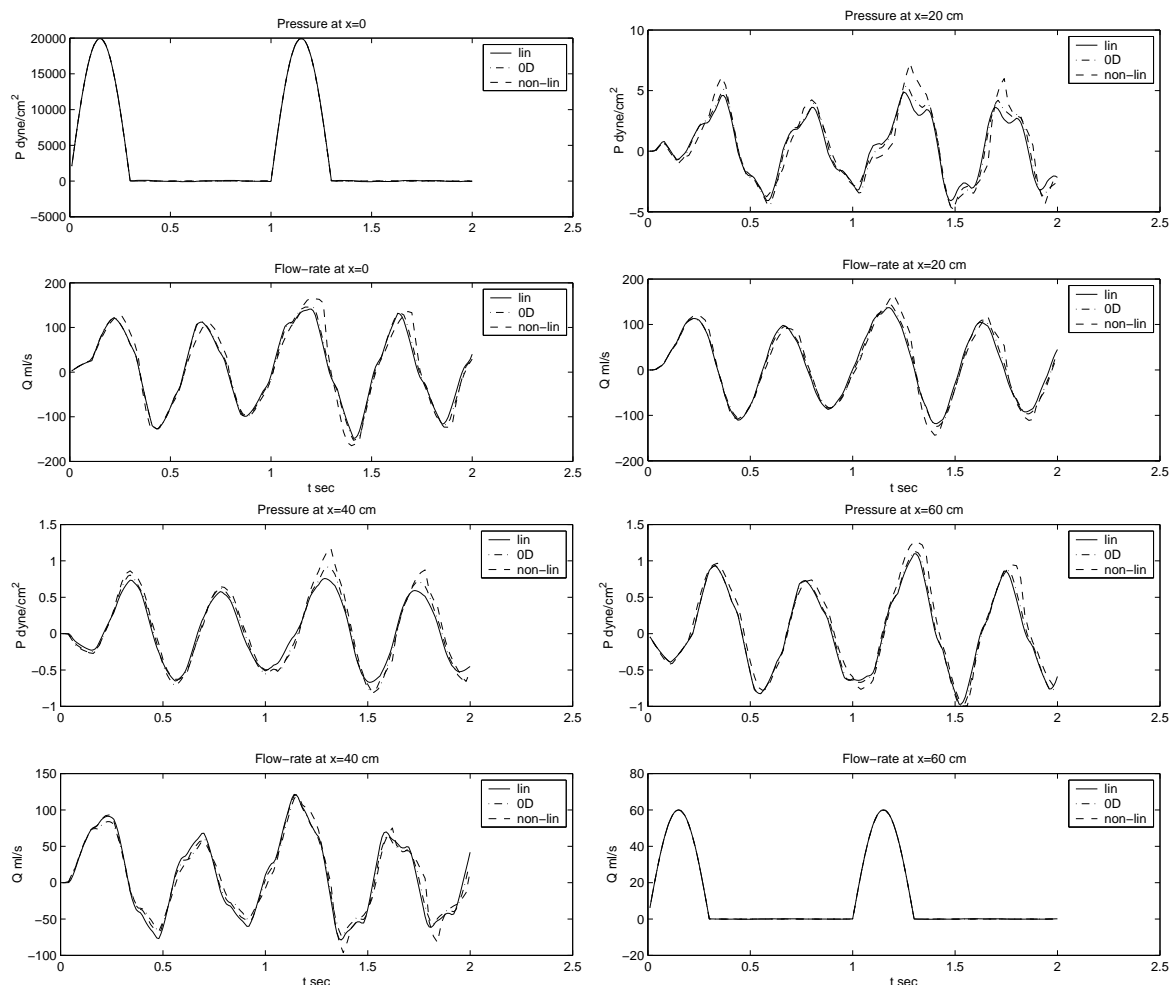


FIGURE 3. Display of numerical solutions at four different locations in space: linear 1D model, 0D network (50 elements), nonlinear 1D model

the scheme (43) is stable and its solution tends toward the solution of the following hyperbolic system

$$\begin{cases} C' \partial_t P + \partial_x Q = -\frac{P}{G'} \\ L' \partial_t Q + \partial_x P = -R' Q \end{cases}$$

Again the same matrix can be used to diagonalize the system, the same norm can be applied to obtain energy estimates. Moreover, we should discretize this system using the same techniques as in section 2.4.2 providing new and efficient numerical schemes.

2.6.2. The sleeve effect

To deal with a large vessel, axial averaging could turn to be a rough approximation. We may deduce a more realistic model by considering the vessel as a set of cylindrical shells or annular elements (see figure 5.a). In this way the transversal average is not taken over the whole section but over n concentric annuli, reducing

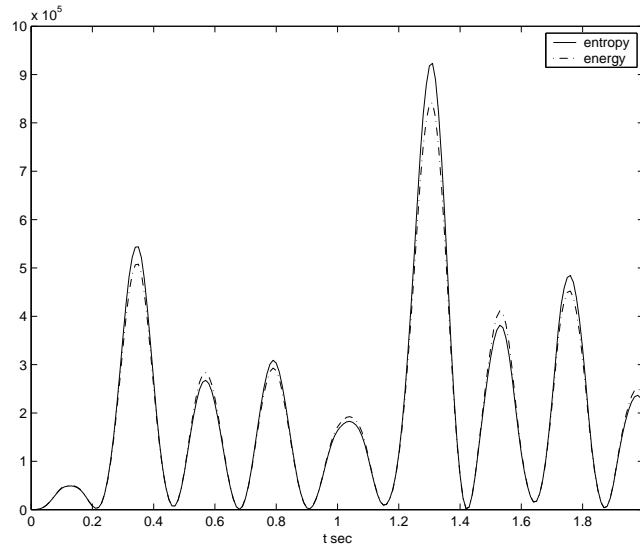


FIGURE 4. Comparison between linear energy E_{Δ} and a discrete version of \mathcal{E} in time

the associated approximation error, see [14, 20, 10]. The resulting model can still be interpreted as an electric network as illustrated in figure 5.b.

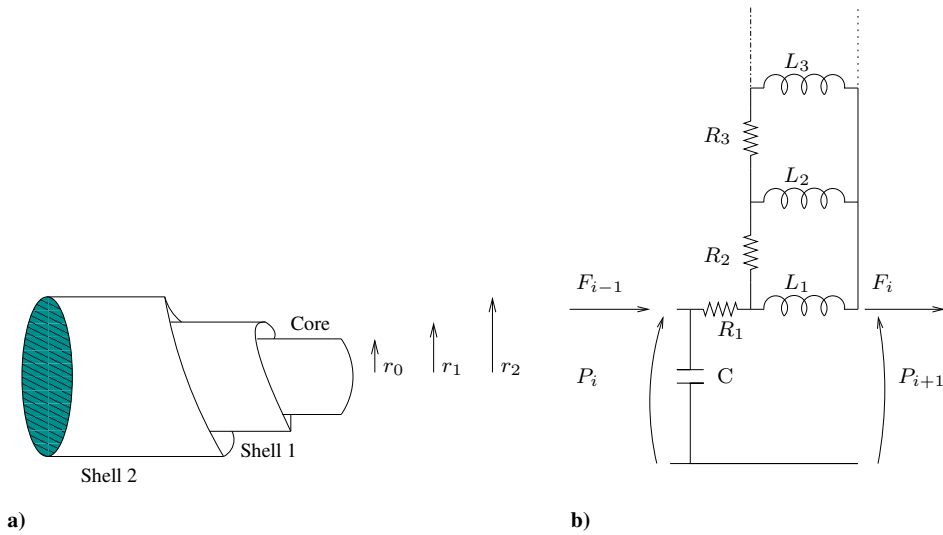


FIGURE 5. Representation of a cylindrical vessel as a set of concentric cylindrical shells, and its corresponding electric network

Applying Kirchhoff's laws one can derive the ODE system that models the general electric network with n resistors R_i and n inductances L_i . Then under a suitable CFL condition, its forward Euler discretization

converges as $\Delta t, \Delta x$ tend to zero toward the following $n \times n$ hyperbolic system:

$$\begin{cases} C' \partial_t P + \partial_x Q = 0 \\ L'_1 \partial_t F_1 + \partial_x P = -R'_1 Q \\ L'_2 \partial_t F_2 + \partial_x P = -R'_1 Q - R'_2(Q - F_1) \\ L'_3 \partial_t F_3 + \partial_x P = -R'_1 Q - R'_2(Q - F_1) - R'_3(Q - F_1 - F_2) \\ \vdots \\ L'_i \partial_t F_i + \partial_x P = -\sum_{j=1}^i R'_j \left(Q - \sum_{k=1}^j F_k \right) = -\sum_{j=1}^n \left(\sum_{k=1}^{\min(i,j)} R_k \right) F_j \end{cases}$$

for $i = \{1, \dots, n\}$, with $Q = \sum_{i=1}^n F_i$. The primed quantities being as previously adimensionalized with respect to the vessel's length.

3. SMALL VESSELS

The micro-circulation network formed by the arterioles, capillaries, as vessels with radii less than (roughly) $100 \mu\text{m}$ is both topologically and functionally different from the network of large and medium size vessels, [24]. At this spatial scale, blood can no longer be considered as a Newtonian fluid. The properties of the flow are strongly influenced by the individual red blood cells it contains in suspension [18]. This affects fluid viscosity (known as Fahraeus effect), flow profiles and distribution of flow at bifurcations. Thus the equations used to model flow through the larger vessels are no longer valid. The large number of micro-circulation networks connecting each small artery to small vein also makes the method of discretely modelling individual vessel segments computationally prohibitive. To overcome this problems, a lumped parameter model of micro-circulation is used [25]. This model contains only a resistor and a capacitance.

3.1. Introducing the underlying equations

In the small vessels it is reasonable to assume that the velocity profile is almost steady so that it solves the Stokes problem. If the vessel is axisymmetric, we can write the equation in cylindric coordinates

$$\begin{cases} \frac{1}{\rho} \partial_x P = \nu \left(\frac{1}{r} \partial_r w + \frac{\partial^2 w}{\partial r^2} + \frac{\partial^2 w}{\partial x^2} \right) \\ \frac{1}{\rho} \partial_r P = \nu \left(\partial_r \left(\frac{1}{r} \partial_r (rv) \right) + \frac{\partial^2 v}{\partial x^2} \right) \end{cases} \quad (44)$$

and suppose the incompressibility condition

$$\partial_r v + \frac{v}{r} + \partial_x w = 0,$$

where v and w are the radial and the axial components of the velocity and r is the radial coordinate. Following the asymptotic reduction already performed in [4], in a more general case, we suppose the following characteristic quantities: V_0 and W_0 are the characteristic radial and axial velocities, λ is the characteristic length, R_0 is the characteristic inner vessel radius, and the corresponding non-dimensional variables read

$$r = R_0 \tilde{r}, \quad x = \lambda \tilde{x}, \quad t = \frac{\lambda}{W_0} \tilde{t}, \quad w = W_0 \tilde{w}, \quad v = V_0 \tilde{v}, \quad P = \rho W_0^2 \tilde{P}.$$

We set $\lambda = \frac{R_0 W_0}{V_0}$ and $\epsilon = \frac{R_0}{\lambda}$ is of order $\mathcal{O}(10^{-2})$ in small vessels. The previous equations become

$$\begin{cases} \frac{\partial}{\partial \tilde{x}} (\tilde{r} \tilde{p}) = \frac{\mu \lambda}{W_0 R_0^2} \left[\frac{\partial}{\partial \tilde{r}} \left(\tilde{r} \frac{\partial \tilde{w}}{\partial \tilde{r}} \right) \right] \\ \frac{\partial \tilde{p}}{\partial \tilde{r}} = 0 \\ \frac{\partial}{\partial \tilde{r}} (\tilde{r} \tilde{v}) + \frac{\partial}{\partial \tilde{x}} (\tilde{r} \tilde{w}) = 0 \end{cases} \quad (45)$$

where we have neglected terms of order greater than 1 in ϵ . The second equation in (45) implies that the pressure is constant on each cross-section, that's why we only introduce the averaged axial velocity

$$\tilde{\underline{u}} = \frac{1}{\tilde{R}^2} \int_0^{\tilde{R}} 2\tilde{w}\tilde{r}d\tilde{r}$$

where \tilde{R} is the inner vessel radius in the adimensional variables. Integrating the incompressibility equation in the radial direction and using the standard streamline condition :

$$\frac{d\tilde{R}}{dt}(x, t) = \frac{\partial \tilde{R}}{\partial \tilde{t}} + \tilde{w} \frac{\partial \tilde{R}}{\partial \tilde{x}} = \tilde{v},$$

we obtain

$$\frac{\partial}{\partial \tilde{t}} \tilde{R}^2 + \frac{\partial}{\partial \tilde{x}} (\tilde{R}^2 \tilde{\underline{u}}) = 0.$$

In the same way, the first momentum equation becomes :

$$\int_0^{\tilde{R}} \tilde{r} \partial_{\tilde{x}} P d\tilde{r} = \frac{\mu \lambda}{W_0 R_0^2} \tilde{R} [\partial_{\tilde{r}} \tilde{w}]_{\tilde{r}=\tilde{R}}$$

If we define the dimensional axial velocity by

$$\underline{u} = \frac{1}{R^2} \int_0^R 2rw dr,$$

we obtain that $\underline{u} = W_0 \tilde{\underline{u}}$. This gives finally in the dimensional variables

$$\begin{cases} \partial_t A + \partial_x Q = 0 \\ \frac{A}{\rho} \partial_x P = 2\pi \nu R [\partial_r w]_{r=R}. \end{cases} \quad (46)$$

where the A is the cross-section area of the vessel, and $Q = A\underline{u}$ is the flow-rate. To close the system we assume the typical velocity profile

$$w = \frac{\gamma + 2}{\gamma} \underline{u} \left[1 - \left(\frac{r}{R} \right)^\gamma \right],$$

(here this is very reasonable because the flow is almost steady see [32]). Notice that $\gamma = 2$ corresponds to the Newtonian fluid. When $\gamma = 9$ the profile is closed to the plug flow profile. Thanks to this assumption, the right hand-side of the latter equation in (46) becomes

$$f = 2\pi \nu R [\partial_r w]_{r=R} = 2\nu R \left(-\frac{(\gamma + 2)}{R} \underline{u} \right) = -2\nu(\gamma + 2)\underline{u} = -K_r \underline{u}$$

leading to the following nonlinear system

$$\begin{cases} \partial_t A + \partial_x Q = 0 \\ \frac{A}{\rho} \partial_x P = -K_r \frac{Q}{A}. \end{cases} \quad (47)$$

Applying again the strategy used in section 2.1, we express the latter system in the P, Q variables using the closure law (2). Then we linearize around $A = A_0$ to obtain the following system

$$\begin{cases} C' \partial_t P + \partial_x Q = 0 \\ \partial_x P = -R' Q \end{cases} \quad (48)$$

that can be rewritten in a single equation that reads

$$C' \partial_t P - \frac{1}{R'} \partial_{xx} P = 0, \quad t \geq 0. \quad (49)$$

As previously the constants can be defined as in (6) by

$$R' = \frac{\rho K_r}{A_0^2}, \quad C' = \frac{2A_0 \sqrt{A_0}}{\beta}$$

Remark 3.1. A similar linearized law is derived in [5, 3] without assumptions on the profile leading to different definitions of constants R' and C' .

Remark 3.2. System (49) can be seen as the limit equation when the inductance term goes to 0 in (7), when the latter is written as a linear wave equation with a parabolic perturbation

$$L' C' \partial_{tt} P + R' C' \partial_t P - \partial_{xx} P = 0.$$

This shows that there is a coherent approach at every scale of approximation.

In a very standard way, we multiply equation (49) by P and integrate by parts to obtain

$$C' R' \frac{d}{dt} \int_{\mathbb{R}} P^2 dx = - \int_{\mathbb{R}} |\partial_x P|^2 dx \leq 0$$

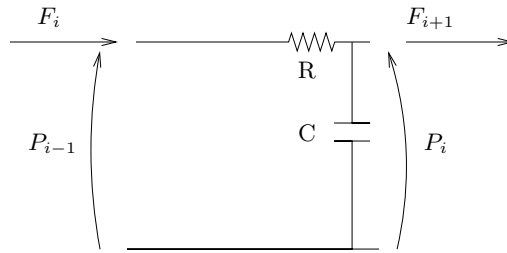
which means that the energy dissipated by this element is bounded, and depends only on the initial and boundary data. Note that the energy functional E_{Δ} introduced in 2.2 degenerates here to a single function of the pressure.

3.2. Discretizing (49) with 0D models

As in section 2.1 we integrate (48) in the axial direction and we suppose the same simplifying assumptions (9). This provides the following ODE system

$$\begin{cases} C \frac{dP_i}{dt} = Q_i - Q_{i+1} \\ R Q_i = P_{i-1} - P_i, \end{cases} \quad (50)$$

that can be regarded again as the mathematical description of an RC -electric circuit like that depicted in figure 3.2.a. Again, we have assumed that $R = R' \Delta x$ and $C = C' \Delta x$ where Δx is the length of a single compartment described by (50). By letting the index i vary from $-\infty$ to $+\infty$, and connecting together the same structure

FIGURE 6. The RC -circuit

for all i , we obtain :

$$C \frac{dP_i}{dt} = Q_i - Q_{i+1} = \frac{1}{R} [P_{i+1} - 2P_i + P_{i-1}], \quad (51)$$

which is a first order discretization (w.r. to Δx) of (49).

If we use the forward Euler scheme to discretize (51) in time, we need the following condition

$$\Delta t \leq \left(\frac{R'C'}{2} \right) \Delta x^2,$$

in order to guarantee stability and therefore convergence toward the solution of the parabolic equation (49).

4. CONCLUSIONS AND PERSPECTIVES

In this paper we have provided a rigorous approach for electric circuits whose physical constants (R, L and C) are parametrized on the actual length of the vessel in order to recover correct values for pressure or flow-rate.

For large and medium sized vessels we have shown the convergence of the lumped parameter model toward the solution of a 1D linear system, that is shown itself to be a linearization of the widely used 1D nonlinear system. Convergence is proven in a norm which derives from the entropy function of the 1D nonlinear system. Energy estimates were already available for the electric networks but no connection were made with 1D hyperbolic systems. Our result can therefore be regarded as a unifying approach for the three hierarchical models based on electric circuits, linear 1D hyperbolic systems and the (more complete) nonlinear 1D hyperbolic system.

This convergence result has prompted us to analyze from a new point of view the numerical features of the RLC -circuits, and underline their major drawbacks: stability of solutions under a “parabolic” CFL condition, the forward Euler discretization of RLC -circuits is bounded but not strictly decreasing (while the continuous problem and the semi-discrete scheme are actually strictly dissipative), the wave propagation is asymmetric. Moreover, this analysis led to propose new lumped parameter models inheriting properties of upwind schemes, that should be furtherly investigated.

The numerical tests have shown a good agreement between the linear energy and the entropy functional on solutions whose order of magnitude corresponds to physiological data. The convergence of the classical RLC -circuits was verified and a comparison between linear and nonlinear solutions of the 1D models was established.

In a second part of this paper, moving from the Stokes equations in an axisymmetric vessel, we have derived the whole hierarchy of equations for small vessels and showed that again RC -circuits converge toward a parabolic equation for the pressure.

The coupling of linear one-dimensional models with appropriate interface conditions is under investigation [17], based on the interface techniques necessary to consider couplings of systems of different kinds, namely between linear hyperbolic and parabolic PDE's, PDE's and ODE's in order to construct multiscale models. The final goal would be the treatment of the nonlinear systems that are currently used for blood flow simulations.

ACKNOWLEDGMENTS

This study was partially supported by the RTN project HaeModel HPRN-CT-2002-00270 and the Bernoulli center at the Ecole Polytechnique Fédérale de Lausanne during the special semester on the “Mathematical Modelling of the Cardiovascular System”. The authors wish to express their thanks to Alessandro Veneziani and Luca Formaggia from M.O.X. of the Politecnico di Milano, for fruitful discussions, and encouragements. The second author also acknowledges the contribution of the research projects MIUR-Cofin 2003 “Advanced Numerical Methods for Applications of Partial Differential Equations” and INDAM “Numerical Analysis for Scientific Computing and Advanced Applications”, 2003.

REFERENCES

- [1] A.P. Avolio. Multibranch model of the human arterial system. *Med. and Biol. Eng. and Comput.*, 18:709 – 119, 1980.
- [2] B. S. Brook, S. A. E. G. Falle, and T. J. Pedley. Numerical solutions for unsteady gravity-driven flows in collapsible tubes: evolution and roll-wave instability of a steady state. *J. Fluid Mech.*, 396:223–256, 1999.
- [3] A. Canic, S. Mikelic and D. Lamponi. Self-consistent effective equations modeling blood flow in medium-to-large compliant arteries. Preprint.
- [4] S. Čanić and E.H. Kim. Mathematical analysis of quasilinear effects in a hyperbolic model of blood flow through compliant axi-symmetric vessels. *Math. Meth. Appl. Sci.*, 26:1161–186, 2003.
- [5] S. Canic and A. Mikelic. Effective equations modeling the flow of a viscous incompressible fluid through a long elastic tube arising in the study of blood flow through small arteries. *SIAM J. Appl. Dyn. Sys.*, 2003.
- [6] L. de Pater and J.W. van den Berg. An electrical analogue of the entire human circulatory system. *Med. Electron. Biol. Engng.*, 2:161–166, 1964.
- [7] C.A. Desoer and E.S. Kuh. *Basic Circuit Theory*. McGraw-Hill, 1969.
- [8] L. Euler. *Principia pro motu sanguinis per arterias determinando. Opera posthuma mathematica et physica anno 1844 detecta.*, volume 2, pages 814–823. 1775.
- [9] L. Formaggia, J. F. Gerbeau, F. Nobile, and A. Quarteroni. On the coupling of 3D and 1D Navier-Stokes equations for flow problems in compliant vessels. *Comput. Methods Appl. Mech. Engrg.*, 191(6-7):561–582, 2001.
- [10] L. Formaggia and A. Veneziani. Reduced and multiscale models for the human cardiovascular system. Technical report, PoliMI, Milan, June 2003. Collection of two lecture notes given at the VKI Lecture Series 2003-07, Brussels 2003.
- [11] O. Frank. Die grundform des arteriellen pulses. erste abhandlung, mathematische analyse. *Z. Biol.*, 37:483–526, 1899.
- [12] E. Godlewski and P.-A. Raviart. *Hyperbolic systems of conservation laws*. Mathématiques & Applications [Mathematics and Applications], 3/4. Ellipses, Paris, 1991.
- [13] S. Hales. *Statical essays containing haemostatics*, volume 2. Innys and Manby, London, 1733.
- [14] G.N. Jager, N. Westerhof, and A. Noordegraf. Oscillatory flow impedance in electrical analog of the arterial system. *Circ. Res.*, 16:121–133, 1965.
- [15] W.P. Mason. *Electromechanical Transducers and Wave Filters*. 1942.
- [16] F. Migliavacca, G. Pennati, G. Dubini, R. Fumero, R. Pietrabissa, G. Urcelay, E.L. Bove, T.Y. Hsia, and M.R. de Leval. Modeling of the norwood circulation: effects of shunt size, vascular resistances, and heart rate. *Am. J. Physiol. Heart Circ. Physiol.*, 280(5):H2076–H2086, May 2001.
- [17] V. Milišić and A. Quarteroni. Coupling between linear parabolic and hyperbolic systems of equations for blood flow simulations. Work in preparation.
- [18] A. R. Pries, D. Neuhaus, and P. Gaetgens. Blood viscosity in tube flow: dependence on diameter and hematocrit. *Am. J. Physiol.*, 263:1770–1778, 1992.
- [19] A. Quarteroni, R. Sacco, and F. Saleri. *Numerical Mathematics*, volume 37 of *Texts in Applied Mathematics*. Springer-Verlag, New York, 2000.
- [20] V.C. Rideout and D.E. Dick. Difference-differential equations for fluid flow in distensible tubes. *IEEE Trans. Biomed. Eng.*, BME-14(3):171–177, 1967.
- [21] P. Segers, F. Dubois, D. De Wachter, and Verdonck P. Role and relevancy of a cardiovascular simulator. *J Cardiovascular Engineering*, 3:48–56, 1998.
- [22] S.J. Sherwin, V. Franke, J. Peiro, and K. Parker. One-dimensional modelling of a vascular network in space-time variables. *Journal of Engineering Mathematics*, 2003.
- [23] R. Skalak. *The synthesis of a complete circulation, in Cardiovascular Fluid Dynamics*, volume 2, pages 341–376. Academic Press, London, 1972.
- [24] N. P. Smith, A. J. Pullan, and P. J. Hunter. An anatomically based model of transient coronary blood flow in the heart. *SIAM J. Appl. Math.*, 62(3):990–1018 (electronic), 2001/02.
- [25] J.A. Spaan and J.D. Breuls, N.P. Laird. Diastolic-systolic coronary flow differences are caused by intramyocardial pump action in the anesthetized dog. *Circ. Res.*, Sep 49(3):584–593, 1981.

- [26] N. Stergiopoulos, B. E. Westerhof, and N. Westerhof. Total arterial inertance as the fourth element of the windkessel model. *Am. J. Physiol.*, 276:H81–H88, 1999.
- [27] N. Stergiopoulos, D.F. Young, and T.R. Rogge. Computer simulation of arterial flow with applications to arterial and aortic stenoses. *J. Biomech.*, 25:1477–1488, 1992.
- [28] J.C. Stettler, P. Niederer, and M. Anliker. Theoretical analysis of arterial hemodynamics including the influence of bifurcations. part i: Mathematical model and prediction of normal pulse patterns. *Ann. Biomed. Eng.*, 9:145–164, 1981.
- [29] J.C. Strikwerda. *Finite difference schemes and partial differential equations*. The Wadsworth & Brooks/Cole Mathematics Series. Wadsworth & Brooks/Cole Advanced Books & Software, Pacific Grove, CA, 1989.
- [30] N. Westerhof, F. Bosman, C.J. De Vries, and A. Noordergraaf. Analog studies of the human systemic arterial tree. *J. Biomechanics*, 2:121–143, 1969.
- [31] N. Westerhof, G. Elzinga, and P. Sipkema. An artificial system for pumping hearts. *J. Appl. Physiol.*, 31:776–781, 1971.
- [32] F. White. *Viscous Fluid Flow*. McGraw-Hill, 1986.